

Magnetic Mapping for Robot Navigation in Indoor Environments

David Almeida, Eurico Pedrosa, Francisco Curado

Institute of Electronics and Informatics Engineering of Aveiro (IEETA)

Department of Electronics, Telecommunications and Informatics (DETI)

University of Aveiro, 3810-193 Aveiro, Portugal

{dalmeida,efp,fcurado}@ua.pt

Abstract—Magnetic disturbances of the Earth’s magnetic field (magnetic anomalies) occur normally in indoor environments due to the presence of ferromagnetic artefacts, such as reinforced concrete or steel infrastructures and other local metallic objects. In conventional robot navigation, which uses the direction of the Earth’s magnetic field to determine orientation, these anomalies are seen as undesirable. However, if the environment is rich in anomalies with sufficient local variability, these can be mapped and used as features for localization purposes. The work presented here aims at exploiting these magnetic features optimally for navigation of mobile robots, by employing advanced interpolation techniques that permit precise mapping of magnetic fields in indoor environments that cannot be surveyed according to a regular grid during map acquisition and may suffer from large gaps in the magnetic coverage. First, the issues addressed to create a magnetic map are depicted, namely data acquisition, methods of interpolation employed, and map validation processes. Subsequently, the results of multiple localization experiments are presented and discussed.

Index Terms—Robot navigation, localization in indoor environments, magnetic mapping, particle filter.

I. INTRODUCTION

Navigation is a central subject of mobile robotics and refers to how an agent finds its way in an environment. The subject of navigation can be divided into various topics. Two of these topics are mapping and localization. The first refers to how the map is generated from the robot’s sensors, effectively attributing quantities and parameters to spatial regions or points in the environment. The second refers to how the robot uses the map of the environment and its sensors to find its pose in that same environment. Some of the more conventional robotic navigation systems measure the Earth’s magnetic field to determine an orientation. The work presented here aims at taking advantage of the distortion of the Earth’s magnetic field, prevalent in many indoor environments, to determine the position of a mobile robot.

The emergence of GPS came as a solution for many real time localization systems in outdoor environments. However GPS localization is often unreliable and is unsuitable for indoor applications. The more popular alternatives to GPS require the installation of fixed beacons, as well as line-of-sight between them. There are some alternatives that do

This work was funded by National Funds through the FCT - Foundation for Science and Technology in the context of the project UIDB/00127/2020.

978-1-6654-0402-0/21/\$31.00 ©2021 European Union

not require the installation of fixed position sensors, such as LIDAR or vision based systems, but these are usually expensive, complex, and may present privacy concerns [1] [2].

Many indoor environments present diverse magnetic anomalies, due to the distortion of the Earth’s magnetic field by ferromagnetic objects, such as steel and reinforced concrete structures. The intensity of these magnetic anomalies is usually high enough to be detected by a standard magnetometer [3]. If the magnetic map presents a rich diversity of magnetic anomalies, static in time and spread through space with enough local variability, these can be used as features for localization and navigation purposes [4] [5]. One advantage of magnetic field based systems, when compared with other common indoor localization methods, is the price and availability. Most IMUs contain a magnetometer, as well as many common devices, including cellphones. Additionally, since vision is not required, magnetic mapping is interesting in face of privacy concerns; it is also a passive system. An adapted SLAM system could serve as a solution for some domestic appliances (such as robot vacuum cleaners, for example).

The central objective of the work presented here is to precisely map the unique magnetic fingerprint of a two dimensional environment, while resorting to magnetometer measurements and an accurate ground truth positioning system. For this purpose, we employed an advanced interpolation technique named ordinary Kriging, which is widely used in a geostatistical context, but yet to be tested in the context of indoor magnetic mapping for robot navigation purposes. Moreover, the quality of the magnetic map was thoroughly tested with multiple localization experiments, where a localization algorithm, based on a particle filter, estimated the position of a mobile robot in the mapped area, while resorting to wheel odometry, magnetometer measurements and the previously built magnetic map.

The remaining parts of this document aim at: discussing the related work regarding ambient magnetic field mapping and localization; presenting and justifying the employed hardware; thoroughly describing the magnetic mapping process; briefly describing the localization algorithm and discussing the experimental results of the tests performed to evaluate the accuracy and reliability of the navigation system; presenting the conclusions of the paper.

II. RELATED WORK

Despite its paramount importance in terms of the performance of map-based localization systems, as in the case of magnetic based navigation, the problem of mapping the magnetic field of a given environment is a topic scarcely discussed in the literature. A notable exception is the work described in [3] where ambient magnetic fields are modeled and spatially prolonged using Gaussian processes. For such, the authors build on Maxwell equations in order to physically model the underlying magnetic field and apply a Bayesian non-parametric probabilistic modeling technique for interpolation and extrapolation of the field over the area to be mapped. That paper does not address explicitly the localization problem, which the authors have covered in prior work [6].

The work described in [4] employs an equipment with a setup similar to the one used in our work, consisting of a small mobile robot equipped with a single 3-axis magnetometer and odometry sensors. The results reported there, were obtained in an extensive set of experiments (conducted along the corridors of different buildings) and demonstrate the feasibility of achieving a relatively high positioning accuracy (between 0.1 m and 0.7 m of mean estimation error) along extended paths using this simplified setup, provided that a relatively accurate map of the environment has been made available for localization. The robot localization accuracy obtained in those experiments is practically the same when using only the norm of the 3-axis measurement vector or when using its 3 vector components as the observation; this can be explained in part by the one-dimensional nature of the experiment which simplifies the localization problem.

Another work that relies on the utilization of a single MEMs-based tri-axis magnetometer, with characteristics similar to those of our sensor, is reported in [7]; the localization method employs a Rao-Blackwellized Particle Filter (RBPF) for 6D pose estimation based on a dynamical model of the sensor, fed by motion input provided by an Xsens MTi IMU, and vector magnetic measurements acquired with the 3-axis magnetometer of the IMU, which are compared with a 3D magnetic map computed from an analytic model of the ambient magnetic field induced by a magnetic coil. Despite the sub-metric localization error achieved along most of the experiment, the results were obtained at a maximum distance of 0.4 m from the coil and cannot be considered as representative of more demanding, realistic scenarios.

The paper [5] describes an experimental approach that bears great resemblance with our own work as the authors employ the same type of attitude and motion sensor, an Xsens MT IMU installed on an omnidirectional mobile robot and exploit the measurements of its built-in vector magnetometer which are integrated with the robot odometry by a Monte Carlo Localization (MCL) algorithm to estimate its position within an area of approximately 4m by 10m inside a laboratory; the work described includes experiments conducted with a person walking with a wireless variant of the IMU installed on a shoe. The paper compares the results obtained with different

magnetic measurement representations (field magnitude versus vector components) and grid resolutions of the prior map, which was acquired on a regular grid by the mobile robot in automated mode and supported by a Vicon motion capture system for ground-truth positioning. The authors show that the lower resolution maps (10 cm or even 20 cm grids) provided sufficiently accurate localization results. Another interesting conclusion of that work, is the fact that using only the magnitude of the magnetic measurements, instead of using its vector components, does not degrade significantly the localization accuracy; the MMSE of the robot localization using the magnetic field intensity is lower than 9.5 cm.

The results described in [8] were obtained with an array of six vector magnetometers that are used to detect, model, and estimate the heading errors introduced in magnetic measurements by local field disturbances caused by the buildings structures and materials. Based on the data, a heading correction procedure is applied which enables the utilization of the magnetometers for successful localization along a path through several hundred meters inside a building. However, the authors do not provide any metrics of localization accuracy that can be used for a fair assessment of the method's efficacy.

Some works described in the literature employ artificial landmarks placed on the environment at known positions in order to aid the magnetic-based localization system. As an example, an array of six vector magnetometers is employed in [9], where the magnetic measurements are compared with a 3D magnetic map of the environment acquired on a regular grid; magnetic readings made by a mobile robot are complemented with odometry from the encoders and with data from capacitive proximity sensors, relative to fixed landmarks pre-installed on the floor. The authors performed 1D localization tests with this system along a narrow corridor with approximately 50 m, achieving a mean distance error below 0.1 m and error peaks inferior to 0.4 m. In [10] the authors placed strong permanent magnets, configured with distinctive magnetic field patterns at various positions of an indoor environment, in order to facilitate magnetic-based localization of people using smartphones. The authors report achieving mean localization errors lower than 1 m, by using artificial intelligence methods of pattern recognition (SVM and DNN) of magnetic field disturbances.

There are a series of publications describing magnetic-based indoor positioning systems (IPS) that exploit mobile-phone built-in vector magnetometers to map an indoor environment and self-localize a smartphone user inside buildings. Although this approach has shown a high potential for application in indoor environments, the solutions reported in the literature aim at pedestrian localization and do not provide precise position estimates; in general those magnetic IPS rely on broad magnetic signatures or magnetic models of magnetic disturbances of long wavelength (several meters) and, as a consequence, only provide a coarse localization output, such as the identification of the room or corridor where a user's mobile phone is located, or its proximity to pre-mapped landmarks such as pillars and other building structures with conspicuous

magnetic signatures. This is the case of the works of, e.g. [11] [12] [13] [14], and [15].

Some authors resort to fusion of magnetic and opportunistic WiFi sensing for indoor localization of pedestrians. A illustrative example of this approach is described in [16] where the authors report the results obtained with a smartphone-based person odometry and magnetic mapping and localization, combined with RSS fingerprinting and model-based schemes of WiFi localization, thus achieving sub-metric positioning accuracy in distinct public indoor and underground environments. The work presented in [17], explores a solution that exploits WiFi signals only for initialization of the localization system.

In [11] the authors only provide results of correlation between magnetic intensity signatures measured by a mobile-phone with those previously mapped along several tens of meters and with the output of analytic models of the disturbances caused by building ferromagnetic structures; the paper does not describe localization experiments nor presents metrics of positioning accuracy. A more exhaustive study of the potential and limitations of smartphones for magnetic IPS is presented in [18], which describes distinct calibration procedures and methods for mitigation of the intrinsic errors associated with different mobile phone models, as well as the interference of indoor movable objects, among other disturbing effects.

The most recent developments of this type of magnetic IPS rely on machine-learning methods for feature identification and classification; for example, in [19], the authors rely on smartphone-based magnetic readings and person odometry for localization. They report a success rate between 59 % and 80 % of the DNN model at identifying the magnetic signatures along a straight path, but do not present metrics of localization accuracy. In [20] the same authors improve on prior work and compare positioning results obtained with 3 different magnetic map resolutions and report a landmark detection accuracy by the DNN of over 80 % and positioning performances (average accuracy across experiments) ranging from a sub-meter error along a straight corridor to more than 8 m in an atrium. The authors of [17] relied on crowd-sourced smartphone mapping of the magnetic fingerprints available in the indoor environment and resorted to Hidden Markov Model-based unsupervised learning in order to identify the magnetic signatures and localize the user in the indoor space; the reported HMM-based identification accuracy is 96% and the average positioning error is 2.8 m.

III. WORKSPACE AND EMPLOYED HARDWARE

The magnetometer used in the work presented in this paper was the one incorporated in the MTi-30 AHRS, which is a full gyro-enhanced Attitude and Heading Reference System (AHRS), manufactured by Xsens. The output of the magnetometer is in arbitrary units (a.u.), where one a.u. is the magnetic field strength during calibration at the Xsens calibration lab and corresponds to approximately 40 uT. Figure 1 shows two IMUs installed on the robot, each with a magnetometer, which was the only sensor of the IMU that was used. In the

context of this work, only the data acquired by the bottom IMU was considered. The results of an acquisition with the MTi-30 AHRS in a fixed position, through a period of 24 hours and at a sampling frequency of 1 Hz, are summarized in Table I, and indicate that the MTi-30 AHRS has a good enough precision to be employed in the navigation system.

TABLE I
STATISTICS OF ACQUISITION WITH A FIXED MTI-30 AHRS DURING A 24 HOUR PERIOD.

Statistic	Value
Mean value	1.241 a.u.
Standard deviation	5.110e-3 a.u.
Variance	2.611e-5 a.u. ²
Range of measurements	1.205 a.u to 1.275 a.u.

Both for mapping the ambient magnetic field and experimentally validating the navigation system, an accurate ground truth positioning system is essential. For this purpose, the LMS100 2D LIDAR sensor was used; this sensor was developed to measure distances and scan indoor environments. The raw data outputed by the LIDAR was processed and supplied to a navigation algorithm, in order to provide an accurate estimation of the robot's current pose. The robot has four omnidirectional wheels. Each wheel has an encoder that measures the angular velocity of the wheel. The encoder measurements (also referred as odometry measurements) are then processed to give a dead reckoning estimation of the robot's pose.

The robot's structure is made out of aluminum, which is a non-ferromagnetic material. Nevertheless, the structure may cause some distortion of the ambient magnetic field, since it is an electrically conductive material and can generate induced currents in the presence of strong electromagnetic fields. Furthermore, ferromagnetic impurities may be present in the aluminum alloy. Considering that the strength of the magnetic field, caused by a dipole at a given distance, is inversely proportional to the cube of that same distance [21], the magnetometer has been placed sufficiently far from the vehicle body and other sources of electromagnetic noise, such as engines, in order to mitigate those inferences. In the performed experiments, with the robot in different orientations and in motion, no significant changes were observed in the magnetic field measured by the magnetometer installed in the robot, so it is assumed that there are no distortions caused by the vehicle. Moreover, since the environment was an open field (Figure 2), the bottom IMU was placed as close to the ground as possible, ensuring that it was the closest to the magnetic anomalies caused by the ferromagnetic structures bellow the building's floor.

IV. MAGNETIC MAPPING METHODOLOGY

A. Magnetic Data Acquisition and Processing

Along the data acquisition process, there were three key values that were registered: the magnetometer measurements, the ground truth position and the wheel odometry measurements. These measurements were synchronized and acquired

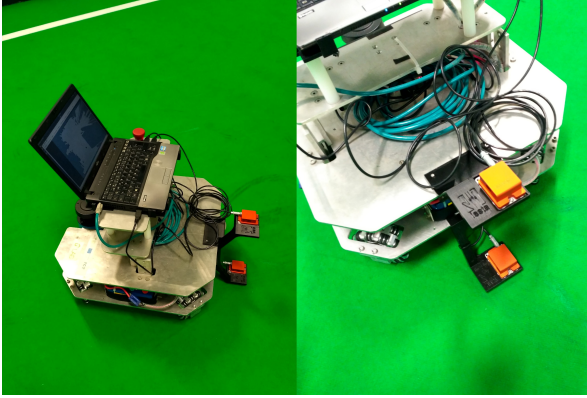


Fig. 1. The two MTi-30 AHRS (only the bottom one was used).



Fig. 2. Workspace

at a sampling frequency of 50 Hz. The mapped area has dimensions of 11.5 m by 8.9 m. Figure 3 shows the trajectory performed by the magnetometer during the mapping acquisition. The mobile robot was controlled remotely and manually, while trying to follow a pre-defined path in the form of a lawn-mower trajectory (in order to obtain a dense coverage of the area). It should be noted that the data collected along the vertical lines (parallel to the ordinate axis) was acquired first, followed by the horizontal lines (parallel to the abscissa axis) that intersect the vertical lines. Figure 4 presents the norm of the magnetic field vector acquired during the same trajectory. The maximum and minimum magnetic intensity measurements acquired during this phase were 5.275 a.u. and 0.018 a.u., respectively.

To validate the acquisition, the measurements taken in the same region, at separate times, were compared and verified to have similar values. The colored dots in Figure 5 represent the intersections in the robot's mapping trajectory. The color spectrum indicates the absolute difference between the two measurements taken at each intersection, at different times. Between most of the samples that are compared at each intersection, a significant amount of time has passed and

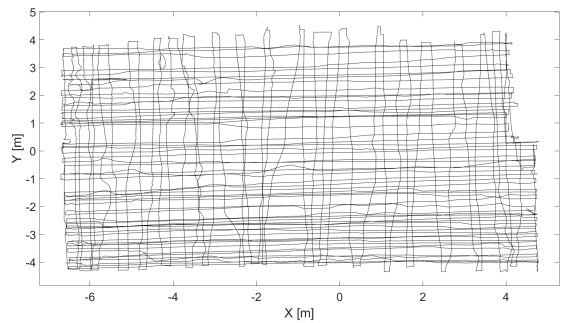


Fig. 3. Robot's trajectory while acquiring data to map the workspace.

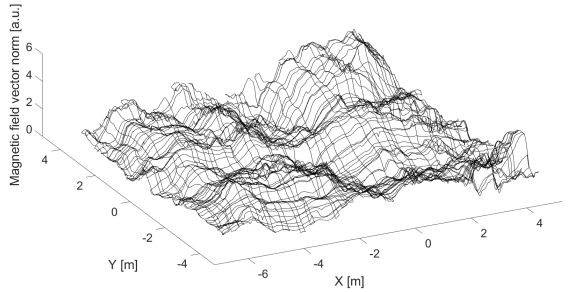


Fig. 4. Magnetometer measurements throughout mapping trajectory.

the robot has covered a considerable distance. Since the acquisition was performed with a sampling rate of 50Hz and the speed of the robot was considerably slow (when compared with the sampling frequency), the samples compared at each intersection were sufficiently close to each other. Considering the 2382 intersections registered, the mean of the absolute difference at each intersection was 0.031 a.u. The maximum absolute difference was 0.192 a.u. and only 32 intersections registered a an absolute difference higher than 0.1 a.u.

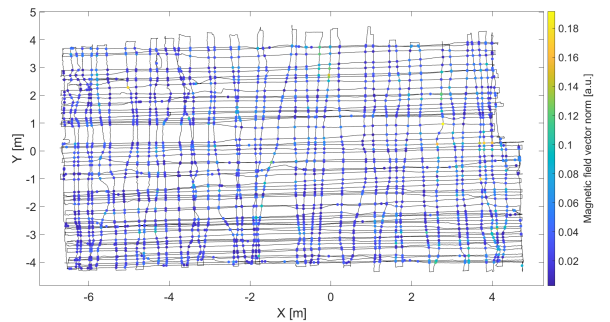


Fig. 5. Mapping trajectory with colored dots representing the registered intersections where the magnetometer measurements were compared. The color spectrum indicates the absolute difference between the two measurements taken at each intersection.

B. Magnetic Data Interpolation

After performing an acquisition on the area to be mapped, the next step was to interpolate the data to a grid of points

regularly distributed throughout the map. The points where the magnetic field vector norm was interpolated formed a 0.02 m by 0.02 m square grid, throughout the entirety of the map. The computational method used to interpolate the data was ordinary Kriging. Kriging is a geostatistical interpolation method that uses the spatial correlation of the distance and direction between the points where measurements have been taken (often called sample points and whose value is represented by Z_s). If the process is second order stationary and follows a normal distribution, ordinary Kriging will be the optimal predictor [22]. This condition is in accordance with the nature of magnetic field strength data. Moreover, in cases where mapping on a regular and dense grid is unfeasible (due to the presence of obstacles, for example), Kriging is best suited for precise interpolation than other more conventional methods (like bilinear interpolation). The value at the interpolated points (also called grid points, in this context, whose value is represented by Z_g) are calculated through Equation (1) [23].

$$Z_g = \sum_{n=1}^N w_k[n] Z_s[n] \quad (1)$$

The value interpolated at each grid point is based on the values at the sample points in the search area near the grid point. This search area is usually delimited by a circumference with a specified radius, with its center on the grid point. In the performed interpolation, a radius of 7.1 meters was used. In this context, w_k denotes the weights that are multiplied by the value at the sample points to estimate the value at the grid points. Thus, each sample point in the search neighborhood of a certain grid point, has a specific weight, whose value is usually inversely proportional to the distance between the sample and grid points. The higher the weight of a sample point, the more influence its value will have on estimating the value of the grid point. In order to optimize the interpolation, the weights used in this method must be computed from variograms (or semi-variograms), which are a mathematical model of the continuity of spatial data. Figure 6 presents a variogram of the acquired data. The abscissa axis of the variogram is the lag distance, which represents the distance between each of the sample points. The Y axis represents the average absolute difference (in a.u.), for each lag distance. To obtain a variogram function, the data must be fitted to a defined function. In this case, a spherical fitting was employed, with a scale of 0.6 and a length of 2.1 meters.

The weights for each sample point are calculated through Equation (2), where A is a matrix comprised of variogram functions between each of the sample points in search area, and b is a vector, also comprised of variogram functions, but between the grid point and the sample points in the search area. Equation (3) shows the composition of the matrices, where x_1 to x_n are the grid points in the search neighborhood, x_0 is the grid point, γ is the variogram function and μ the Lagrange parameter [23].

$$Aw_k = b \quad \Leftrightarrow \quad w_k = A^{-1}b \quad (2)$$

$$\begin{bmatrix} w_{k_1} \\ \vdots \\ w_{k_n} \\ \mu \end{bmatrix} = \begin{bmatrix} \gamma(x_1 - x_1) & \dots & \gamma(x_1 - x_n) & 1 \\ \vdots & \ddots & \vdots & \vdots \\ \gamma(x_n - x_1) & \dots & \gamma(x_n - x_n) & 1 \\ 1 & \dots & 1 & 0 \end{bmatrix}^{-1} \begin{bmatrix} \gamma(x_1 - x_0) \\ \vdots \\ \gamma(x_n - x_0) \end{bmatrix} \quad (3)$$

Figure 7 shows the contour map of the interpolated data, which presents some linear alignments of magnetic anomalies that traverse the whole mapped area. These features, which initially were suspected to be artifacts introduced by some deficiency in the signal processing of the magnetic data, were finally identified as being originated by building structures underlying the pavement of the indoor environment. Thus, instead of constituting undesirable artifacts, these are useful features from the point of view of magnetic navigation because they constitute important sources of information in terms of localization.

In order to validate the quality of the interpolation, additional data was acquired on some of the interpolated regions, after the interpolation had already been performed. As was already mentioned, the magnetic data was interpolated to a 0.02 m by 0.02 m square grid. To obtain an interpolated value at the position of each of the sample points of the post mapping trajectories, a bilinear interpolation was applied, using the four closest grid points. The colored dots in Figure 8 represent the samples taken in three separate trajectories. The color spectrum indicates the absolute difference between the measured value of each sample and the interpolated value at the position of that same sample. Considering the 21334 samples, the mean of the absolute difference between the interpolated and acquired values was 0.0262 a.u. The maximum absolute difference was registered at 0.630 a.u. While most values are within the uncertainty of the magnetometer, some greater discrepancies correspond to regions where the gradient of the magnetic field is higher, and where errors in the ground truth positioning often result in a greater difference between the interpolated and acquired magnetic field intensity values. Table II summarizes some of the results presented up to this point.

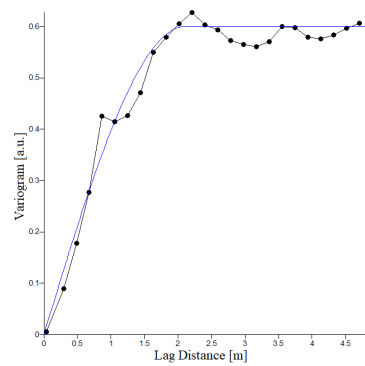


Fig. 6. Example of variogram of mapping acquisition with spherical fitting.

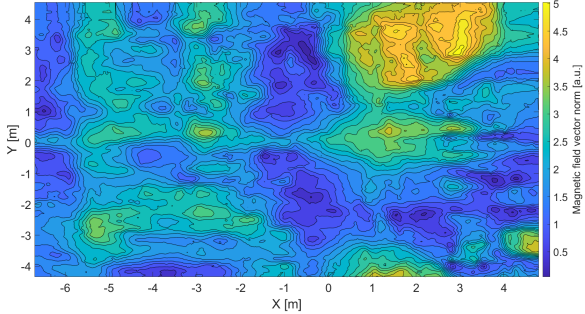


Fig. 7. Magnetic contour map of interpolated data.

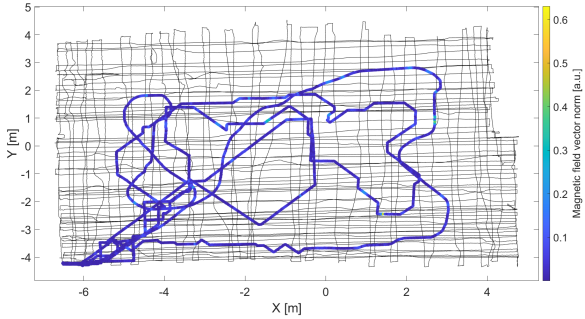


Fig. 8. Validation of the interpolated map by comparing the data acquired in three separate trajectories (colored dots) with the interpolated data. The color spectrum indicates the absolute difference between the measured value of each sample and the interpolated value at the position of that same sample.

V. EXPERIMENTS AND RESULTS

In order to assess the quality of the interpolated magnetic map and its suitability for robot navigation, a localization algorithm, based on a particle filter, was developed and implemented in MATLAB R2019b. The role of the algorithm was to continuously estimate the robot's position, while the robot is performing an arbitrary trajectory on the mapped area. In order to give an estimation of the robot's current position, the algorithm relied on the previously built magnetic map, as well as the magnetometer and wheel odometry measurements. Subsequently, a series of experiments were performed, where the algorithm's estimated position was compared with the ground truth position.

The developed localization algorithm is based on the Monte Carlo Localization algorithm [24]. It is a popular and easy to implement algorithm, which represents the robot's belief $bel(X_t)$ by particles [25], [26]. Apart from the initial particle distribution, the algorithm has four main phases: prediction, importance weighing, state estimation and resampling. Regarding the initial particle distribution, if there is absolutely no knowledge of the robots initial position, the particles are uniformly distributed throughout the map and the center of the map is assumed to be the starting position. However, if the robot's actual starting position is supplied to the algorithm, the particles will follow a Gaussian distribution with mean equal to the initial ground truth position. The resampling phase

TABLE II
STATISTICS OF RESULTS FROM MAPPING PHASE.

Statistic	Value
Standard deviation of acquisition with a static magnetometer through a 24 hour period	5.110e-3 a.u.
Variance of acquisition with a static magnetometer through a 24 hour period	2.611e-5 a.u. ²
Range of measurements acquired during mapping trajectory	0.018 a.u. to 5.275 a.u.
Mean of absolute differences registered in validating the acquisition	0.0311 a.u.
Standard deviation of absolute difference registered in validating the acquisition	0.0221 a.u.
Variance of absolute difference registered in validating the acquisition	4.869e-04 a.u. ²
Mean of absolute difference registered in validating the interpolation	0.0262 a.u.
Standard deviation of absolute difference registered in validating the interpolation	0.0347 a.u.
Variance of absolute difference registered in validating the interpolation	1.207e-3 a.u. ²

is controlled by the number of effective samples N_{eff} [27], which provides an estimate on how well the current particles represent the true estimate [28].

Figure 9 shows the ground truth position, the position given only by the processed odometry measurements and the position estimated by the particle filter, for a test where the particle filter was supplied with the starting ground truth position. In this experiment the initial particle distribution followed a Gaussian distribution, with mean equal to the ground truth position. As the robot travels more distance, the position given by the odometry gradually drifts from the ground-truth position. Clearly, the particle filter was able to successfully correct the cumulative error given by the odometry.

Figures 10 through 12 show the ground truth and estimated positions, for three different trajectories, where the particle filter was not supplied with the starting ground truth position. In each experiment, the particles were uniformly distributed throughout the map and the center of the map was assumed to be the starting position. The filter's estimation was able to converge to a position close to the ground truth on all tests. As expected under these circumstances, the position given only by the odometry measurements presents significant error and is even temporally off the map's limits.

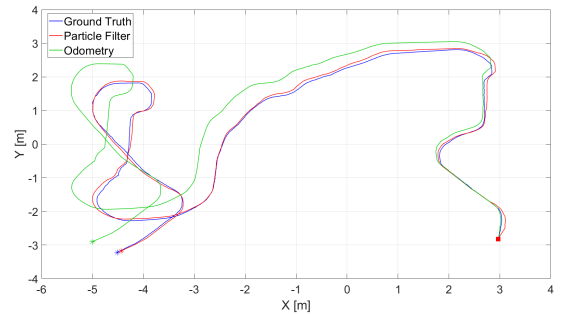


Fig. 9. Particle filter estimated trajectories of test with a known starting position and no initial positioning error.

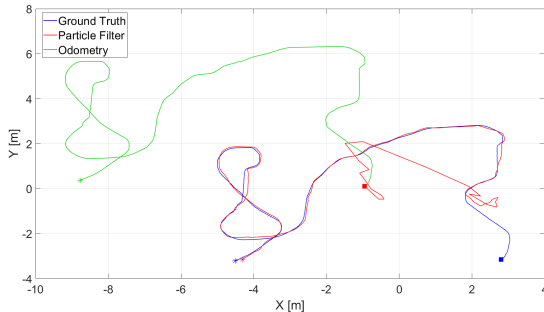


Fig. 10. Particle filter estimated trajectories of first test with an unknown starting position and uniformly distributed particles.

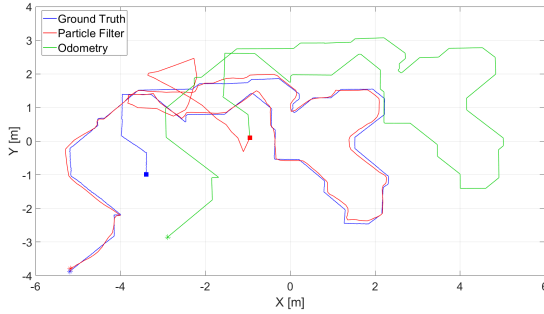


Fig. 11. Particle filter estimated trajectories of second test with an unknown starting position and uniformly distributed particles.

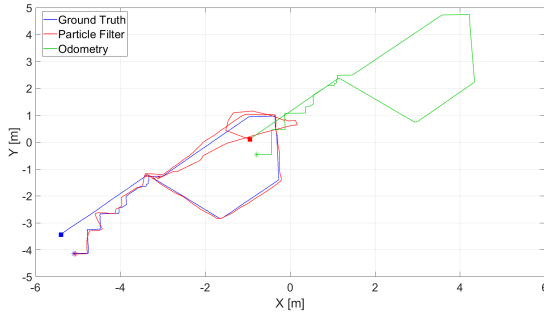


Fig. 12. Particle filter estimated trajectories of third test with an unknown starting position and uniformly distributed particles.

A. Monte Carlo Experiments

In order to test the accuracy and reliability of the navigation system, three Monte Carlo experiments were performed, each consisting of 1000 simulations, with the data portrayed in Figures 10 through 12. For each simulation, an initial new set of particles was randomly generated. Figures 13 through 15 present the evolution of the particle filter estimation error for all simulations of the three Monte Carlo experiments, each corresponding to a different acquisition (previously portrayed in Figures 10 through 12, respectively). Every time the ground truth positioning indicated that the robot had moved an additional 0.1 meters, the particle filter positioning error was

determined by calculating the distance between the position estimated by the particle filter and the ground truth position at that time. From a total of 3000 simulations, the particle filter estimation successfully converged to the ground truth position in 2998 simulations. The point of convergence was considered to be the first point where the particle filter error dropped below 0.1 meters. On each Monte Carlo experiment, after convergence, the behaviour of the error function was similar on all simulations. Table III summarizes the results of the Monte Carlo experiments with an unknown starting position and uniformly distributed particles, where the reported errors are the post-convergence errors.

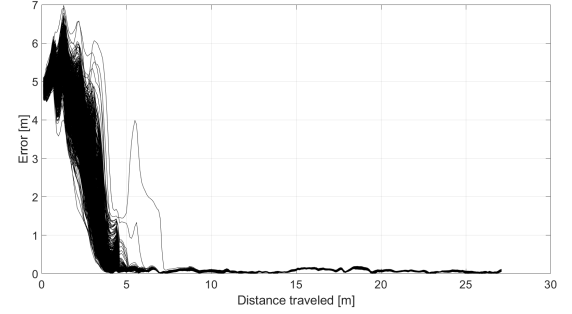


Fig. 13. Evolution of particle filter estimation error for 1000 simulations of the first test with unknown starting state.

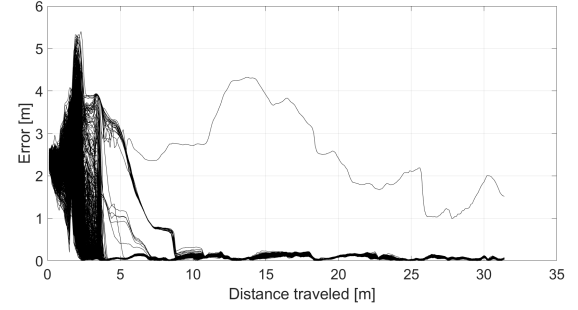


Fig. 14. Evolution of the particle filter estimation error for 1000 simulations of second test with an unknown starting state.

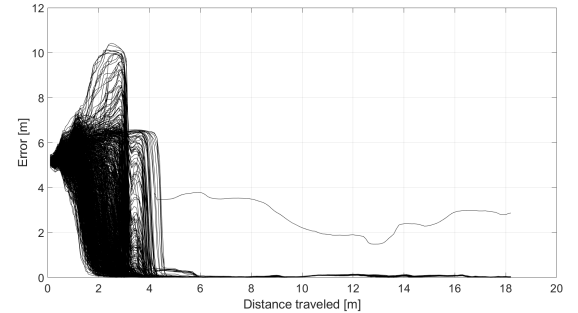


Fig. 15. Evolution of the particle filter estimation error for 1000 simulations of third test with an unknown starting state.

TABLE III

RESULTS OF MONTE CARLO EXPERIMENTS WITH AN UNKNOWN STARTING POSITION AND UNIFORMLY DISTRIBUTED PARTICLES.

Result description	Value
Nº of converging simulations for 1st test	1000 out of 1000
Mean of particle filter error for 1st test	0.068 m
Maximum of particle filter error for 1st test	0.196 m
Nº of converging simulations for 2nd test	999 out of 1000
Mean of particle filter error for 2nd test	0.083 m
Maximum particle filter error for 2nd test	0.209 m
Nº of converging simulations for 3rd test	999 out of 1000
Mean of particle filter error for 3rd test	0.070 m
Maximum of particle filter error for 3rd test	0.188 m

VI. CONCLUSION

In this work we study particularly the topic of precise magnetic mapping of indoor environments for the purpose of magnetic-based localization and propose a new, more robust and accurate method for this task. The process followed to create and validate the magnetic map was thoroughly characterized, since a good magnetic map is as important as an accurate localization algorithm. The interpolation method adopted to create the magnetic map was ordinary Kriging, which is broadly used in a geostatistical context. However, this interpolation method was yet to be tested in the context of indoor magnetic mapping for robot navigation.

The experiments performed indicate that the developed navigation system is reliable and accurate enough to address many indoor localization problems. Out of all experiments where the algorithm's estimation was able to converge to the ground truth position, a mean positioning error of less than 10 centimeters was registered (after the particle filter had converged). Moreover, regarding the experiments where the localization algorithm was not supplied with the robot's initial position, the filter was able to successfully converge to the ground truth position on 2998 out of 3000 simulations.

In conclusion, the results are encouraging and demonstrate that it is possible to achieve a localization accurate enough to solve many mobile robot navigation problems using magnetic data. The magnetic mapping process was tested and shown to be suitable for indoor robot navigation. Nevertheless, magnetic field based localization systems are dependant on the magnetic features of the environment and there needs to be more work done in order to further test the reliability of these types of systems. This implies performing more tests in different environments and under diverse conditions.

REFERENCES

- [1] F. Zafari, A. Gkelias, and K. K. Leung, "A survey of indoor localization systems and technologies," *IEEE Communications Surveys Tutorials*, vol. 21, no. 3, pp. 2568–2599, 2019.
- [2] W. Sakpere, M. Adeyeye Oshin, and N. Mlitwa, "A state-of-the-art survey of indoor positioning and navigation systems and technologies," *South African Computer Journal*, vol. 29, p. 145, 12 2017.
- [3] A. Solin, M. Kok, N. Wahlström, T. B. Schön, and S. Särkkä, "Modeling and interpolation of the ambient magnetic field by gaussian processes," *IEEE Trans. on Robotics*, vol. 34, no. 4, pp. 1112–1127, 2018.
- [4] J. Haverinen and A. Kemppainen, "Global indoor self-localization based on the ambient magnetic field," *Robotics and Autonomous Systems*, vol. 57, no. 10, pp. 1028–1035, 2009.
- [5] M. Frassl, M. Angermann, M. Lichtenstern, P. Robertson, B. J. Julian, and M. Doniec, "Magnetic maps of indoor environments for precise localization of legged and non-legged locomotion," in *Intelligent Robots and Systems (IROS), 2013 IEEE/RSJ International Conference on*, 2013, Conference Proceedings, pp. 913–920, printed.
- [6] A. Solin, S. Sarkka, J. Kannala, and E. Rahtu, "Terrain navigation in the magnetic landscape: Particle filtering for indoor positioning," in *2016 European Navigation Conference (ENC)*, 2016, pp. 1–9.
- [7] M. Kok, N. Wahlström, T. B. Schön, and F. Gustafsson, "Mems-based inertial navigation based on a magnetic field map," in *IEEE International Conference on Acoustics, Speech and Signal Processing (ICASSP), 2013*, 2013, Conference Proceedings, pp. 6466–6470.
- [8] M. H. Afzal, V. Renaudin, and G. Lachapelle, "Assessment of indoor magnetic field anomalies using multiple magnetometers," in *Institute of Navigation GNSS Conference. ON GNSS 2010, Session F1, Portland, Oregon, 21-24 September 2010*, Conference Proceedings.
- [9] H.-S. Kim, W. Seo, and K.-R. Baek, "Article indoor positioning system using magnetic field map navigation and an encoder system," *Sensors* 2017, vol. 17, no. 651, pp. 1–16, 2017.
- [10] E. Fisher, A. Ivy, R. Alimi, and E. Weiss, "Smartphone based indoor localization using permanent magnets and artificial intelligence for pattern recognition," vol. 11, no. 015122 (2021).
- [11] B. Gozick, K. P. Subbu, R. Dantu, and T. Maeshiro, "Magnetic maps for indoor navigation," *IEEE TRANSACTIONS ON INSTRUMENTATION AND MEASUREMENT*, vol. 60, no. 12, 2011.
- [12] K. P. Subbu, B. Gozick, and R. Dantu, "Locateme: Magnetic-fields-based indoor localization using smartphones," vol. 4, no. 4, pp. 1–27, 2013.
- [13] C. Galván-Tejada, J. P. García-Vázquez, and R. F. Brena, "Magnetic field feature extraction and selection for indoor location estimation," *Sensors*, vol. 14, pp. 11 001–11 015, 2014.
- [14] I. Ashraf, S. Hur, and Y. Park, "Enhancing performance of magnetic field based indoor localization using magnetic patterns from multiple smartphones," vol. 20, no. 2704, 2020.
- [15] L. Fernandes, S. Santos, M. Barandas, D. Folgado, R. Leonardo, R. Santos, A. Carreiro, and H. Gamboa, "An infrastructure-free magnetic-based indoor positioning system with deep learning," vol. 20, no. 6664, 2020.
- [16] Y. Shu, C. Bo, G. Shen, C. Zhao, L. Li, and F. Zhao, "Magicol: Indoor localization using pervasive magnetic field and opportunistic wifi sensing," *IEEE Journal on Selected Areas in Communications*, vol. 33, no. 7, Jul. 2015.
- [17] M. Kwak, C. Hamm, S. Park, and T. T. Kwon, "Magnetic field based indoor localization system: A crowdsourcing approach," in *Int. Conf. on Indoor Positioning and Indoor Navigation (IPIN)*, 2019, pp. 1–8.
- [18] D. Vandermeulen, C. Vercauteren, and M. Weyn, "Indoor localization using a magnetic flux density map of a building - feasibility study of geomagnetic indoor localization," in *Int. Conf. on Ambient Computing, Applications, Services and Technologies*, 2013, Conference Proceedings.
- [19] N. Lee and D. Han, "Magnetic indoor positioning system using deep neural network," in *2017 International Conference on Indoor Positioning and Indoor Navigation (IPIN)*, 2017, pp. 1–8.
- [20] N. Lee, S. Ahn, and D. Han, "Amid: Accurate magnetic indoor localization using deep learning," vol. 18, no. 1598, 2018.
- [21] J. D. Jackson, *Classical Electrodynamics Third Edition*. John Wiley & Sons Inc, 1998.
- [22] J.-S. Ryu, M. Kim, K. Cha, T. Lee, and D.-H. Choi, "Kriging interpolation methods in geostatistics and dace model," *KSME International Journal*, vol. 16, pp. 619–632, 05 2002.
- [23] H. Wackernagel, *Multivariate Geostatistics*. Springer, 1995.
- [24] D. F. Sebastian Thrun, Wolfram Burgard, *Probabilistic Robotics*. The MIT Press, 2000.
- [25] Z. Chen, "Bayesian filtering: From kalman filters to particle filters, and beyond," *Statistics*, vol. 182, 01 2003.
- [26] E. Pedrosa, A. Pereira, and N. Lau, "Fast grid slam based on particle filter with scan matching and multithreading," pp. 194–199, 2020.
- [27] N. Kwak, I. Kim, H. Lee, and B. Lee, "Analysis of Resampling Process for the Particle Depletion Problem in FastSLAM," in *RO-MAN 2007 - The 16th IEEE International Symposium on Robot and Human Interactive Communication*, Aug. 2007, pp. 200–205.
- [28] J. S. Liu, "Metropolized independent sampling with comparisons to rejection sampling and importance sampling," *Stat. Comput.*, vol. 6, no. 2, pp. 113–119, Jun. 1996.